Structural study of Zn and Cd to ultrahigh pressures

Takemura Kenichi*
National Institute for Research in Inorganic Materials, Namiki 1-1, Tsukuba, Ibaraki 305, Japan
(Received 3 September 1996; revised manuscript received 16 January 1997)

High-pressure powder x-ray diffraction experiments on Zn and Cd have been carried out at room temperature to above 100 GPa with high precision. Both metals remain in the hcp structure up to the highest pressures investigated (126 GPa for Zn and 174 GPa for Cd). The c/a axial ratios continuously decrease with pressure down to a value of 1.59. We have observed a clear change in the slope of the volume dependence of the axial ratio at $c/a=\sqrt{3}$ for both metals. The anomaly may be related to the electronic topological transition observed in the Mössbauer study on Zn under pressure at low temperature, but the special value ($\sqrt{3}$) of the axial ratio is difficult to explain simply by the electronic topological transition. The hcp structure with the axial ratio of $\sqrt{3}$ has unique symmetry both in real and reciprocal spaces. This suggests a universal change in the bonding properties of the hcp structure at $c/a=\sqrt{3}$. The bulk modulus and its pressure derivative of Zn and Cd have been determined over a large pressure range. [S0163-1829(97)03633-3]

I. INTRODUCTION

Zinc and cadmium have unusually large c/a axial ratios for the hcp structure under ambient conditions ($c/a=1.856$ for Zn and 1.886 for Cd). The model of hard-sphere packing defines the c/a axial ratio for the ideal hexagonal close-packed structure to be $\sqrt{8/3}$ ($\cong 1.6330$). Most of the hcp metals have axial ratios close to this value. The deviation of the axial ratios of Zn and Cd from the ideal value can be explained by the reduction in the band structure energy through lattice distortion.[1–4] Pressure affects the axial ratios, from which one can get insight into the change in the band structures of these highly anisotropic metals under pressure. Structural change of the two metals under pressure is itself of fundamental crystallographic interest.

The effect of pressure on the crystal structures of Zn and Cd was first studied by Lynch and Drickamer[5] and by Perez-Albuerne *et al.*[6] They reported unusual changes in the c/a axial ratios with pressure. The axial ratios decrease with pressure, reach a minimum, and increase. After passing through a broad maximum ($\sim$ 7 GPa for Zn and $\sim$ 10 GPa for Cd) the axial ratios decrease again. Lynch and Drickamer also measured the electrical resistance of these metals and found anomalies in the same pressure ranges.[5] They explained the observations with the pressure-induced change in the topology of the Fermi surface based on the theories proposed by Jones[7] and by Goodenough.[8] McWhan also measured the lattice parameters of Zn and Cd under pressure.[9] He did not find any anomaly in either metal up to 10 GPa, and set an upper limit for the anomaly in the lattice parameters at 0.3%. In 1991, Schulte, Nikolaenko, and Holzapfel carried out an energy-dispersive x-ray diffraction study on Zn and Cd up to about 40 GPa.[10] They reported that the axial ratios of these metals decrease monotonically with pressure and show no anomalies contrary to the results by Lynch and Drickamer. The same conclusion was drawn in a subsequent work on Zn and Cd up to 75 GPa by the same group.[11] From a theoretical side, Meenakshi *et al.* have calculated the equilibrium axial ratio of Zn under high pressure with the use of the linear-muffin-tin orbital (LMTO) method within the atomic-sphere approximation, and found that the volume dependence of the axial ratio changes slope around the relative volume of 0.92.[12] They argued that the anomaly may possibly be related to the maximum of the electronic density of states at the Fermi level.

In 1995, Potzel *et al.* have detected an anomaly in the Mössbauer spectra of Zn at $\sim$ 6.6 GPa and 4.2 K.[13,14] The anomaly is accompanied with a drastic change of the lattice dynamics. Based on the scalar-relativistic linear augmented plane wave calculation, they proposed that the anomaly is related to the topological change of the Fermi surface, the electronic topological transition (ETT). According to their calculation the ETT occurs when the unoccupied band at the L symmetry point drops below the Fermi level under pressure. Soon after the Mössbauer measurements, Takemura carried out a high-pressure x-ray diffraction study on Zn and reported a change in the slope of the volume dependence of the axial ratio at $c/a=\sqrt{3}$ at room temperature ($P=9.1$ GPa, $V/V_0=0.893$).[15] The axial ratio of Zn decreases more rapidly with pressure after it takes the value of $\sqrt{3}$. He discussed the origin of the anomaly by comparing it with the results of the Mössbauer measurements.[13] The axial ratio of Zn at the anomaly in the Mössbauer spectra ($\sim$ 6.6 GPa and 4.2 K) was estimated to be $c/a=1.73\pm0.01$, which agrees with $c/a=\sqrt{3}$ within the estimation error.[15] The two anomalies are therefore possibly correlated, and could be induced by the change in the topology of the Fermi surface, as Potzel *et al.* pointed out. It is, however, difficult to assume that the ETT occurs exactly when the axial ratio takes a special value of $\sqrt{3}$. We briefly discuss the reason as follows.

The ETT occurs when a new Fermi surface appears or an existing Fermi surface disappears.[16] For a simple metal like Zn, the topology of the Fermi surface is basically determined by the size of the Fermi sphere and that of the Brillouin zone boundaries. They are simply calculated based on the nearly-free-electron approximation.[17] A divalent hcp metal has the Fermi sphere expanding into the fourth Brillouin zone. The size of the Fermi sphere and that of the Brillouin zone boundaries are calculated as a function of the c/a axial ratio.

It follows that the Fermi surface changes topology only when the axial ratio takes a value of $27\sqrt{3}/8\pi$ ($\cong 1.8607$).[18] Namely, the nearly-free-electron model does not support the ETT occurring at $c/a=\sqrt{3}$ ($\cong 1.7321$). The actual Fermi surface is of course different from the free-electron picture,[19] making it more difficult to correlate the ETT with the anomaly at $c/a=\sqrt{3}$.

In the present paper we report on the full details of the high-pressure x-ray diffraction experiments on Zn and Cd. We show that the anomaly previously found for Zn also exists for Cd at the same axial ratio of $\sqrt{3}$. This finding strongly suggests that the anomaly in the volume dependence of the axial ratio at $c/a=\sqrt{3}$ is a universal feature for the hcp structure and is not necessarily connected with the ETT. We discuss the interesting symmetry of the hcp structure at $c/a=\sqrt{3}$ both in real and reciprocal spaces. This further suggests that the hcp structures having axial ratios larger and smaller than $\sqrt{3}$ can be classified into two different groups. The present paper provides comprehensive structural data for Zn and Cd to ultrahigh pressures, which serve as a basis for theoretical studies. Part of the present work has been reported elsewhere.[20]

II. EXPERIMENTS

Angle-dispersive powder x-ray diffraction experiments have been carried out under high pressure using a diamond anvil cell (DAC), synchrotron radiation, and an imaging plate. We used the synchrotron radiation on the beam lines 6B (bending magnet), 14C (vertical wiggler), and 18C (bending magnet) of the Photon Factory, National Laboratory for High Energy Physics (KEK). The x ray was monochromatized to 18.00 keV for the experiments on the beam lines 6B and 18C, and 32.57 keV for those on the beam line 14C. Details of the experimental setup and the data analysis have been described elsewhere.[21] A fine powder of Zn (99% purity) with an average particle size of 4 μm was obtained from Rare Metallic Co., Ltd. A powder of Cd (99.9998% purity) with an average particle size of 45 μm was obtained from Koch Chemicals, Ltd. The Cd specimen was etched in dilute HNO_3 solution in order to remove surface oxides.

For the pressure generation we used several kinds of diamond anvils depending on the pressure range. At low pressures flat diamond anvils with 600 μm culet size were used. For ultrahigh pressures we used beveled diamond anvils with 150 μm anvil flat, 300 μm total culet size, and a bevel angle of 7°. The gasket materials were spring steel (PK and GIN6, Hitachi Metals Ltd.) in the case of Zn, and rhenium in the case of Cd, with initial thickness of 200–250 μm. For ultrahigh pressures the gasket was preindented to a thickness of 33 μm, and a hole with 35 μm diameter was made by using a micro electro-discharge machine (MG-ED71, Panasonic). The Zn or Cd sample was enclosed in the gasket hole together with fine ruby powder as a pressure marker, and a methanol-ethanol-water mixture (16:3:1 by volume) as a pressure transmitting medium.[22] The pressure was determined on the basis of the ruby pressure scale.[23] At pressures above 100 GPa, the ruby luminescence was so weak that the pressure was estimated from the d spacings of the gasket. The uncertainty in pressure was $\pm$ 5–10 GPa in this case.

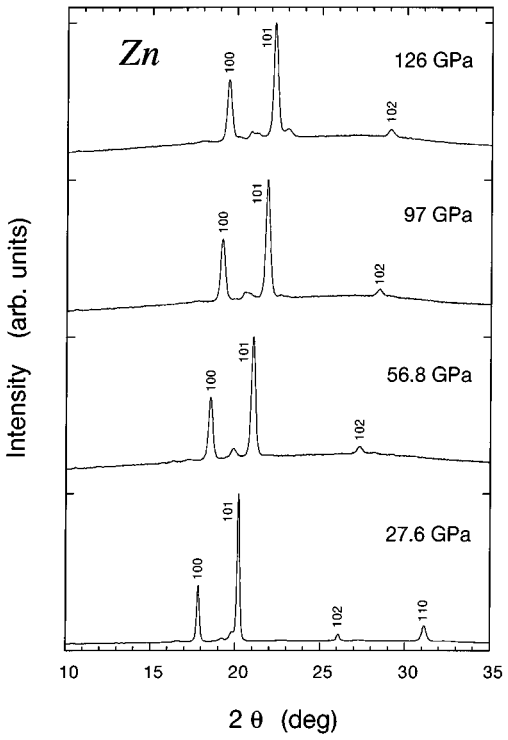

FIG. 1. Powder x-ray diffraction patterns of Zn over a large pressure range. The x-ray energy was 18.00 keV. Weak unindexed peaks are of ZnO formed on the surface of Zn powder. The 002 reflection is not observed due to the preferred orientation.

In total five experimental runs were done for Zn, and three for Cd, in order to check reproducibility. All the diffraction experiments were done at room temperature. Typical exposure times were 1.5 h.

III. RESULTS

Figures 1 and 2 show representative x-ray diffraction patterns of Zn and Cd over wide pressure ranges. Zn and Cd are stable in the hcp structure up to the highest pressures of 126 $\pm$ 3 GPa and 174 $\pm$ 7 GPa, respectively. One notices progressive broadening of diffraction peaks at high pressures, which is caused by the increasing pressure gradient. At low pressures the peak width is small enough to allow one to determine the lattice parameters with high precision. Figures 3 and 4 show x-ray diffraction patterns of Zn and Cd in the low pressure region, demonstrating the quality of peak resolution. The lattice parameters a and c are determined by a least-squares method. For the pressure range of up to 20 GPa, we used 10–17 reflections on average. The observed and calculated d spacings are in excellent agreement to within $\pm$ 0.04%.

Tables I and II summarize the structural data of Zn and Cd under high pressure. Figures 5 and 6 show the pressure dependence of the lattice parameters of Zn and Cd. The c axis is very compressible at low pressures, while at higher pressures the c axis compressibility becomes comparable to that of the a axis. Consequently the c/a axial ratios rapidly decrease in the initial stage of compression and saturate at higher pressures (Fig. 7). It should be noted that the axial

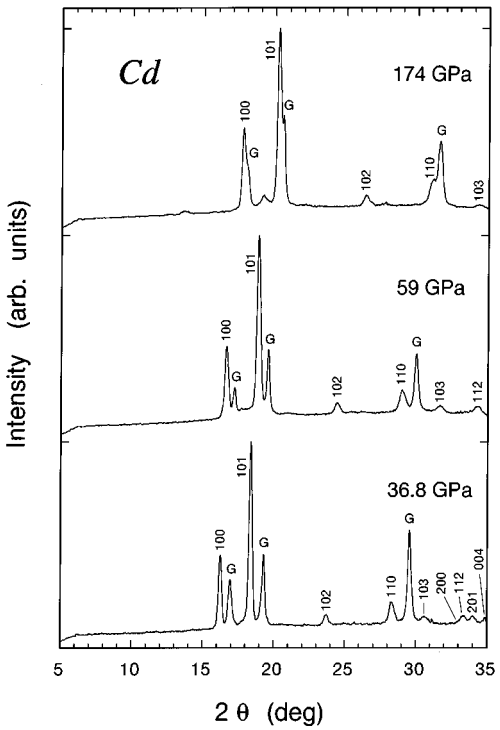

FIG. 2. Powder x-ray diffraction patterns of Cd over a large pressure range. The x-ray energy was 18.00 keV. Diffraction peaks from the gasket material (Re) are labeled *G*. Other unindexed peaks are of CdO formed on the surface of Cd powder. The 002 reflection is not observed due to the preferred orientation.

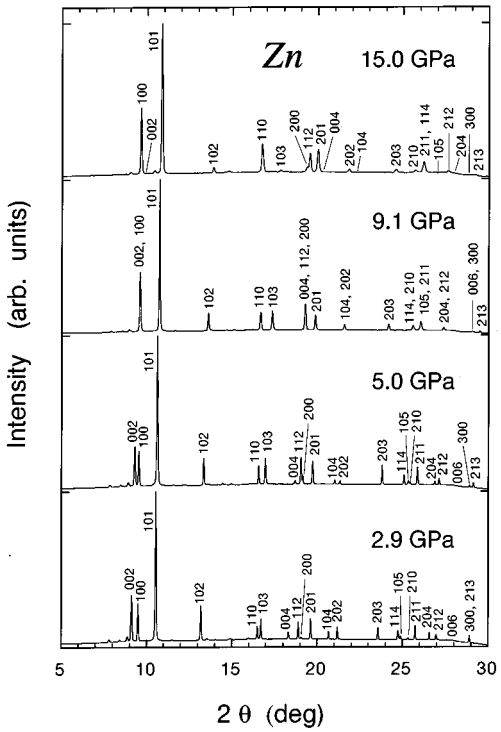

FIG. 3. Powder x-ray diffraction patterns of Zn at low pressures. The x-ray energy was 32.57 keV. Weak unindexed peaks are of ZnO formed on the surface of Zn powder. Notice that a number of diffraction peaks overlap in the pattern at 9.1 GPa.

ratios pass through the ideal value of 1.633 and keep decreasing with increasing pressure. This clearly demonstrates the failure of the naive expectation that the axial ratio always approaches the ideal value at high pressures. The axial ratios of both metals approach a value of 1.59 at the highest pressures. For the study of delicate changes in the axial ratios, it is better to plot the axial ratios as a function of the relative volume V/V_0, where V_0 denotes the volume of each metal at atmospheric pressure (Fig. 8). This kind of plot is free from the uncertainty in pressure determination. Now one notices clear changes in the slope of the volume dependence of the axial ratios at a common value of $\sqrt{3}$. The anomaly exactly corresponds to the point at which many diffraction peaks simultaneously overlap (see the pattern at 9.1 GPa in Fig. 3 and that at 12.2 GPa in Fig. 4). The experimental locations of the anomalies are $V/V_0 = 0.886 \pm 0.002$, $P = 9.4 \pm 0.3$ GPa, and $c/a = 1.733 \pm 0.002$ for Zn, and $V/V_0 = 0.850 \pm 0.002$, $P = 12.5 \pm 0.3$ GPa, and $c/a = 1.732 \pm 0.002$ for Cd.

It is interesting to see whether the a or c axis is responsible for the anomaly in the c/a ratio. Figures 9 and 10 show the pressure dependence of the a and c axis of Zn and Cd in the low pressure region. Notice that the scale for the a axis is expanded ten times that of the c axis. In these figures the data taken under slightly nonhydrostatic conditions are also shown for a comparison.[25] It is evident that the a axis shows anomalous behavior in both cases of Zn and Cd. Particularly in the case of Zn, the a axis slightly *expands* with pressure on the high-pressure side of the anomaly. The anomaly is less clear in the nonhydrostatic runs.

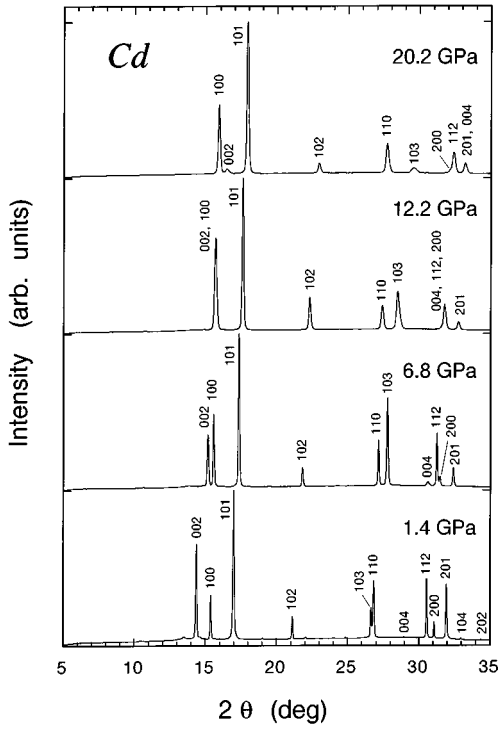

FIG. 4. Powder x-ray diffraction patterns of Cd at low pressures. The x-ray energy was 18.00 keV. Weak unindexed peaks are of CdO formed on the surface of Cd powder. Notice that a number of diffraction peaks overlap in the pattern at 12.2 GPa.

TABLE I. Structural data of Zn under high pressure. The lattice parameters and the axial ratio at normal pressure are taken from Ref. 24 and are $a=2.6644(3)$ Å, $c=4.9454(3)$ Å, and $c/a=1.8561(2)$. The errors in a, c, c/a, and V/V_0 given in parentheses are from least-squares fits.

P (GPa)	a (Å)	c (Å)	c/a	V/V_0
0.2(1)	2.6641(1)	4.9310(3)	1.8509(1)	0.9969(1)
2.0(1)	2.6548(1)	4.8086(3)	1.8113(1)	0.9653(1)
3.5(1)	2.6459(2)	4.7549(5)	1.7971(2)	0.9481(2)
5.5(1)	2.6368(2)	4.6786(6)	1.7743(3)	0.9266(2)
7.2(1)	2.6283(2)	4.6199(4)	1.7578(2)	0.9090(2)
8.5(1)	2.6230(1)	4.5801(1)	1.7462(1)	0.8976(1)
9.5(1)	2.6186(1)	4.5501(3)	1.7376(1)	0.8887(1)
10.4(1)	2.6196(3)	4.5190(7)	1.7250(3)	0.8833(2)
11.7(1)	2.6212(8)	4.4733(20)	1.7066(9)	0.8754(1)
13.1(1)	2.6184(8)	4.4381(18)	1.6950(8)	0.8667(6)
14.2(1)	2.6144(4)	4.4025(10)	1.6839(5)	0.8571(4)
16.0(1)	2.6088(3)	4.3658(6)	1.6735(3)	0.8463(2)
17.4(2)	2.6037(4)	4.3346(10)	1.6648(5)	0.8370(3)
18.5(2)	2.5997(5)	4.3179(12)	1.6609(6)	0.8313(4)
19.8(2)	2.5942(2)	4.3084(5)	1.6608(3)	0.8259(2)
27.6(2)	2.5653(1)	4.1992(7)	1.6369(3)	0.7871(2)
31.4(3)	2.5565(5)	4.1819(20)	1.6358(9)	0.7785(4)
36.5(2)	2.5348(3)	4.1193(12)	1.6251(5)	0.7539(3)
45.1(1)	2.5082(3)	4.0533(14)	1.6160(6)	0.7263(3)
48.0(1)	2.4963(18)	4.0524(43)	1.6234(21)	0.7193(13)
51.7(1)	2.4878(4)	4.0102(18)	1.6119(8)	0.7070(4)
56.8(1)	2.4708(17)	3.9866(39)	1.6135(19)	0.6932(12)
60.2(3)	2.4665(4)	3.9662(20)	1.6080(9)	0.6873(4)
66.5(1)	2.4426(16)	3.9256(38)	1.6071(19)	0.6671(11)
77.7(3)	2.4202(19)	3.8809(44)	1.6035(22)	0.6475(12)
88(1)	2.4037(19)	3.8414(43)	1.5981(22)	0.6322(12)
97(1)	2.3720(9)	3.8011(20)	1.6025(10)	0.6092(6)
110(2)	2.3707(11)	3.7873(26)	1.5975(13)	0.6063(7)
118(3)	2.3591(21)	3.7541(47)	1.5913(24)	0.5951(13)
126(3)	2.3436(15)	3.7261(33)	1.5899(17)	0.5829(9)

TABLE II. Structural data of Cd under high pressure. The lattice parameters and the axial ratio at normal pressure are taken from Ref. 24 and are $a=2.9788(4)$ Å, $c=5.6164(6)$ Å, and $c/a=1.8855(3)$. The errors in a, c, c/a, and V/V_0 given in parentheses are from least-squares fits.

P (GPa)	a (Å)	c (Å)	c/a	V/V_0
0.8(1)	2.9717(1)	5.5399(10)	1.8642(3)	0.9817(2)
1.1(1)	2.9703(2)	5.5217(19)	1.8590(6)	0.9776(3)
1.6(1)	2.9668(3)	5.4824(26)	1.8479(9)	0.9683(5)
2.1(1)	2.9634(3)	5.4509(26)	1.8394(9)	0.9605(5)
3.2(1)	2.9544(5)	5.3949(28)	1.8261(10)	0.9449(6)
6.1(1)	2.9367(1)	5.2320(5)	1.7816(2)	0.9054(1)
7.4(1)	2.9283(2)	5.1810(7)	1.7693(3)	0.8915(2)
11.7(2)	2.9037(4)	5.0447(17)	1.7373(6)	0.8535(4)
13.0(2)	2.8979(8)	5.0064(34)	1.7276(13)	0.8436(7)
14.0(2)	2.8943(4)	4.9638(19)	1.7150(7)	0.8344(4)
15.6(2)	2.8898(4)	4.9164(17)	1.7013(6)	0.8239(4)
17.2(1)	2.8845(5)	4.8777(16)	1.6910(6)	0.8144(4)
18.8(1)	2.8788(3)	4.8387(12)	1.6808(5)	0.8047(3)
20.2(1)	2.8742(5)	4.8107(18)	1.6737(7)	0.7975(4)
23.1(1)	2.8624(2)	4.7647(4)	1.6646(2)	0.7833(1)
24.0(8)	2.8553(1)	4.7548(1)	1.6652(1)	0.7779(1)
32.0(5)	2.8237(10)	4.6545(25)	1.6484(11)	0.7447(7)
36.8(5)	2.8131(14)	4.6108(34)	1.6391(15)	0.7321(9)
42.3(8)	2.7887(9)	4.5462(21)	1.6303(9)	0.7094(6)
50.1(1)	2.7651(4)	4.4878(9)	1.6230(4)	0.6885(2)
59(1)	2.7459(1)	4.4596(2)	1.6241(1)	0.6747(1)
66.4(7)	2.7238(3)	4.3934(7)	1.6129(3)	0.6541(2)
70(2)	2.7134(19)	4.3893(46)	1.6176(20)	0.6485(11)
82.3(4)	2.6874(11)	4.3279(25)	1.6104(11)	0.6272(6)
92(3)	2.6758(21)	4.3032(49)	1.6082(22)	0.6182(12)
153(5)	2.5944(14)	4.1451(32)	1.5977(15)	0.5598(7)
174(7)	2.5731(16)	4.0960(37)	1.5919(17)	0.5442(9)

The pressure-volume relationship of Zn and Cd is shown in Figs. 11 and 12, respectively. As shown in the inset to Fig. 11, the pressure-volume relationship of Zn seems to have a small anomaly around 10–14 GPa corresponding to the expansion of the a axis. The anomaly is, however, obscured by the large compression of the c axis and is not quite clear. The bulk modulus B_0 and its pressure derivative at atmospheric pressure B_0' are determined by fitting the P-V data with the Birch-Murnaghan equation of state. We notice that B_0 and B_0' values are dependent upon the pressure range to be fitted. Table III compares B_0 and B_0' values together with those from previous works. If we fit the present data over the whole pressure ranges, we obtain $B_0=65\pm2$ GPa and $B_0'=4.6\pm0.5$ for Zn, and $B_0=42\pm1$ GPa and $B_0'=6.5\pm0.2$ for Cd. The reader is referred to Ref. 11 for general discussion on the variation of B_0 and B_0' induced by the change in the fitting range of pressure and by the use of different types of equation of state.

IV. DISCUSSION

A. Accuracy of the lattice parameters: Effect of nonhydrostaticity and the number of diffraction peaks used in the refinement

Prior to the discussions of the delicate anomaly in the axial ratios, we have to be careful about the effect of nonhydrostaticity on the lattice parameters. Any change in the nonhydrostatic stress in the sample may produce an anomaly in the lattice parameters. In the present experiments we have used a methanol-ethanol-water mixture (16:3:1 by volume) as a pressure transmitting medium. This pressure medium ensures the hydrostaticity up to about 14.5 GPa.[22] In some experimental runs, however, the amount of the pressure medium was not large enough, and the sample seemed to be subjected to small but appreciable nonhydrostatic stress even at lower pressures than the hydrostatic limit. This is obvious in Figs. 9 and 10, where the lattice parameters obtained under nonhydrostatic conditions are always larger than those under hydrostatic conditions by about 0.2%. When a crystal is subjected to nonhydrostatic stress, the interplanar spacings of the planes normal to the stress direction usually contract, and those of the planes parallel to the stress expand.[28] In the

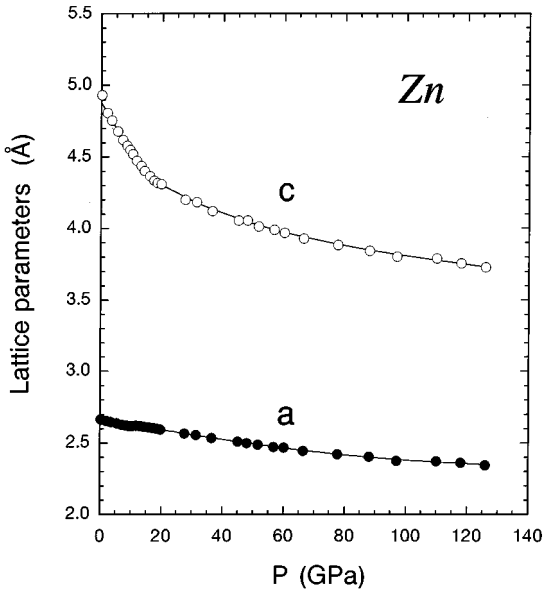

FIG. 5. The lattice parameters of Zn as a function of pressure. The curves are drawn to guide the eyes.

present diffraction geometry with the DAC the x rays are incident on the sample from the direction parallel to the load axis or the stress direction. The x rays are diffracted by lattice planes, which align nearly parallel to the incident x rays (= stress direction) and hence slightly expand under nonhydrostatic stress. In other words, for the present diffraction geometry, the interplanar spacings and the lattice parameters under nonhydrostatic conditions are always observed to be expanded compared with the values under hydrostatic conditions. The axial ratio is, however, less affected by the nonhydrostaticity, since both the a and c axis expand. As a result, the position of the c/a anomaly in the nonhydrostatic case slightly shifts to the high-volume side (Fig. 13), but the

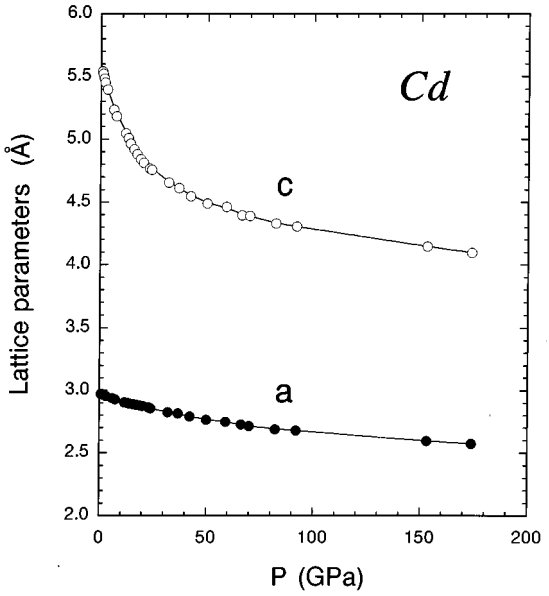

FIG. 6. The lattice parameters of Cd as a function of pressure. The curves are drawn to guide the eyes.

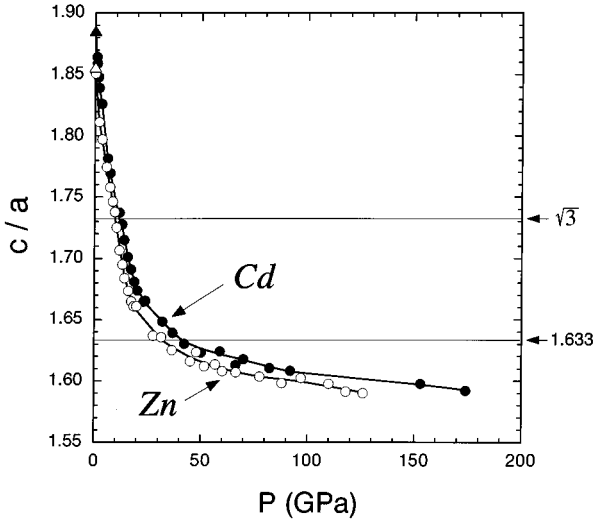

FIG. 7. The change in the axial ratio of Zn and Cd as a function of pressure. Triangles indicate the values at atmospheric pressure from literature (Ref. 24) and circles are from the present work. The curves are drawn to guide the eyes.

value of the critical axial ratio itself ($\sqrt{3}$) remains the same. One notices in Figs. 9, 10, and 13 that the anomalies are more pronounced in the hydrostatic case.

The accuracy of the axial ratio is also affected by the number of diffraction peaks used in the determination of the lattice parameters. Specifically, when several diffraction peaks heavily overlap, their positions are difficult to determine, and hence the total number of reflections valid for the lattice parameter refinement decreases. Since a number of diffraction peaks overlap at $c/a=\sqrt{3}$, it is important to check any systematic influence of the change in the number of reflections. As a test we calculated the lattice parameters of Zn by using nonoverlapping peaks (101, 102, 110, 103, 201, and 203). In this case we also obtain the same anomaly in the

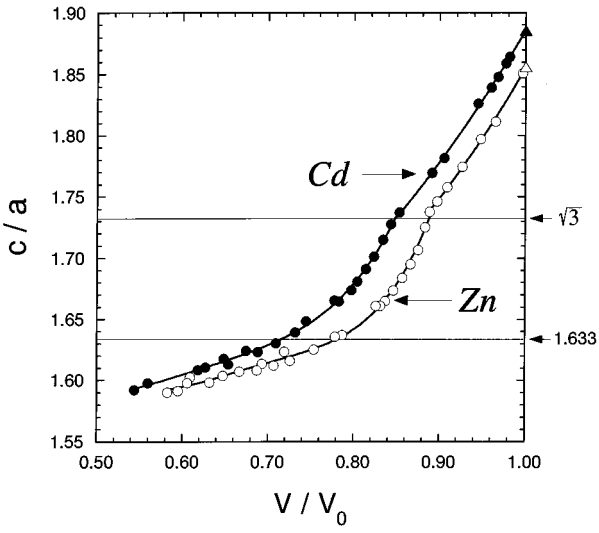

FIG. 8. The change in the axial ratio of Zn and Cd as a function of the relative volume. Triangles indicate the values at atmospheric pressure from literature (Ref. 24) and circles are from the present work. The curves are drawn to guide the eyes.

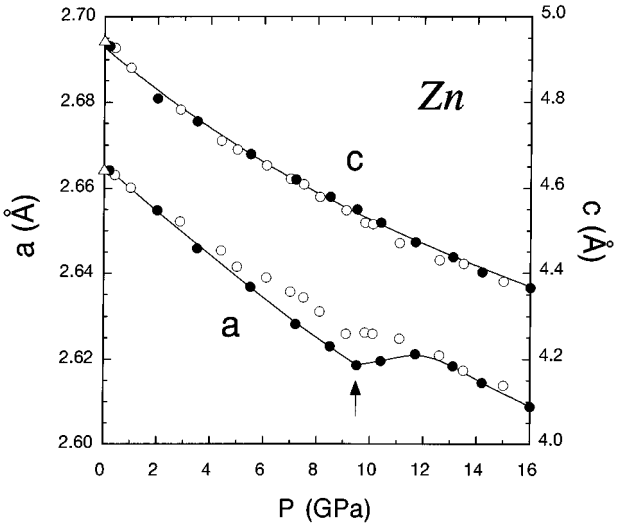

FIG. 9. The lattice parameters of Zn as a function of pressure in the low-pressure region. Triangles indicate the values at atmospheric pressure from literature (Ref. 24) and circles are from the present work. The solid circles indicate the data taken under hydrostatic conditions, and the open circles are from other runs under slightly nonhydrostatic conditions. Notice that the scale for the a axis is expanded ten times that for the c axis. The arrow indicates the anomaly in the a axis. The curves are drawn to guide the eyes.

axial ratio at $c/a=\sqrt{3}$. We conclude that the anomaly is not an artificial effect of the peak overlap occurring at $c/a=\sqrt{3}$. The final values of the lattice parameters are calculated by using more number of reflections as stated in the previous section.

B. Energy band structure, the Fermi surface, and the electronic topological transition in Zn and Cd

In this section we quickly review the electronic properties of Zn and Cd, and discuss the correlation of the c/a anomaly with the ETT expected for these metals under pressure. Zn

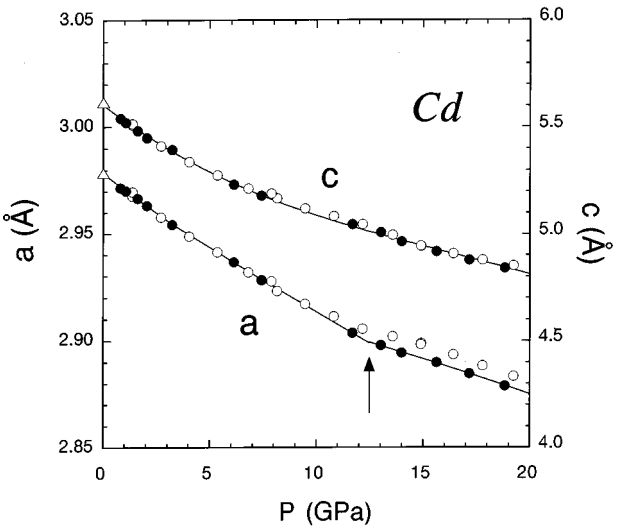

FIG. 10. The lattice parameters of Cd as a function of pressure in the low-pressure region. The notation is the same as in Fig. 9.

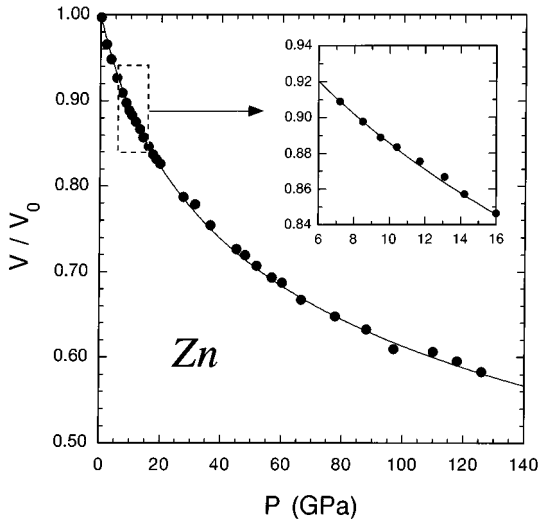

FIG. 11. The pressure-volume relationship of Zn. The solid curve shows a fit with the Birch-Murnaghan equation of state with $B_0 = 65$ GPa and $B_0' = 4.6$. The inset shows an enlarged plot around the c/a anomaly.

and Cd belong to the group IIb elements and are classified into simple sp metals. The basic feature of their band structures can be represented by the nearly-free-electron approximation. Various calculations, however, indicate that the outer core d states ($3d$ of Zn and $4d$ of Cd) lie very close to or above the bottom of the sp conduction bands.[2,4,19,29,30] These d bands make a repulsive contribution to the pseudopotential and significantly modify the conduction band structure. The large c/a axial ratios of Zn and Cd are also explained by the hybridization of the d bands to the conduction bands.[2] For this reason the quantitative discussion of the ETT should be done based on accurate band structure calculations including the d states. Nevertheless, it is still worth doing a simple calculation based on the nearly-free-electron approximation, in order to get a basic idea about the Fermi surfaces of these metals.

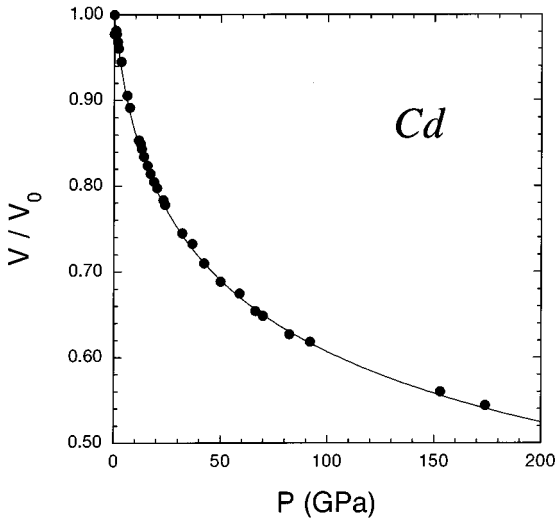

FIG. 12. The pressure-volume relationship of Cd. The solid curve shows a fit with the Birch-Murnaghan equation of state with $B_0 = 42$ GPa and $B_0' = 6.5$.

TABLE III. Bulk moduli and their pressure derivatives of Zn and Cd.

Element	B_0 (GPa)	B_0'	Pressure range (GPa)	Ref.
Zn	59.791	4.880	0–4.5	26
	57 (2)	7.4 (7)	0–8.8	27
	56 (1)	6.6 (3)	0–15	present work
	56 (2)	5 (1)	0–32	10
	63 (2)	5.2 (7)	0–74	11
	65 (2)	4.6 (5)	0–126	present work
Cd	44.76	7.307	0–4.5	26
	48 (1)	5.6 (3)	0–20	present work
	49 (1)	5 (1)	0–40	10
	46 (4)	6.0 (7)	0–68	11
	42 (1)	6.5 (2)	0–174	present work

The Fermi sphere for a divalent hcp metal expands into the fourth Brillouin zone, yielding complicated sheets of Fermi surfaces.[17] They are called ''cap,'' ''monster,'' ''lens,'' ''needles,'' ''butterflies'' (or ''stars''), and ''cigars.''[17,31] The dimension of each sheet is dependent on the c/a axial ratio. Within the nearly-free-electron approximation, Harrison calculated the change in the topology of the Fermi surface for a divalent hcp metal as a function of the axial ratio.[18] It was noted that there is a special value for the axial ratio at which the Fermi sphere crosses the high symmetry point K of the third Brillouin zone, namely, $c/a=27\sqrt{3}/8\pi$ ($\cong 1.8607$). For the axial ratios larger than this value the needles at the K symmetry point disappear. It should be noted that this is the only point at which the topology of the Fermi surface changes in the nearly-free-electron approximation.

The actual Fermi surfaces of Zn and Cd deviate from those predicted by the nearly-free-electron approximation, specifically near the Brillouin zone boundaries. The most prominent difference from the nearly-free-electron approximation is the disappearance of the butterflies and cigars at the L symmetry point both in Zn and Cd.[19,29,32] The existence of the needles at the K symmetry point is controversial.[19]

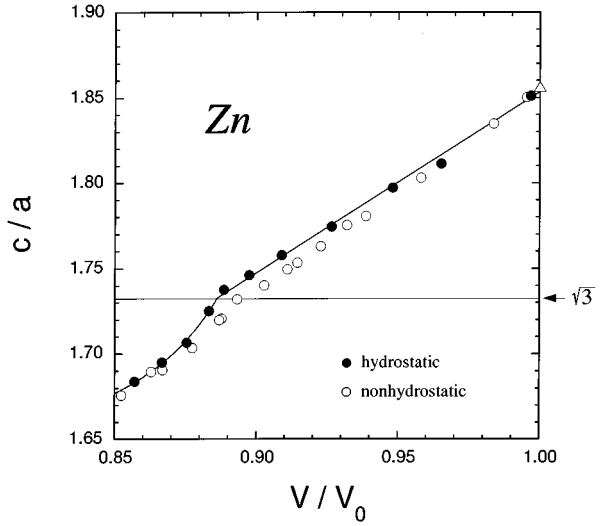

FIG. 13. The change in the axial ratio of Zn as a function of the relative volume in the low-pressure region. The solid circles indicate the data taken under hydrostatic conditions, and the open circles are from other runs under slightly nonhydrostatic conditions. The triangle indicates the value at atmospheric pressure from literature (Ref. 24). The curves are drawn to guide the eyes.

Since the nearly-free-electron approximation indicates that the butterflies at the L symmetry point as well as the needles at the K point increase in size with decreasing c/a ratio, we may expect that these elements eventually appear as the actual Fermi surfaces of Zn and Cd, when the axial ratio decreases under pressure. It should be noted that the ETT has been experimentally identified for Cd under pressure by the measurements of magnetoresistance[33] and the de Haas–van Alphen effect,[34] in which the needles at the K symmetry point are believed to be involved. Newest band-structure calculations employing the LMTO method also show that the ETT occurs at the L, K, and H symmetry points at reduced volumes for Zn and Cd.[35–38] The calculated relative volumes for these ETT's range from 0.9 to 0.8. The axial ratios of Zn and Cd under high pressure are obtained based on the total energy. The calculated volume dependence of the axial ratio shows several anomalies, most of which seem to be correlated with the ETT's. This is reasonable, since any ETT modifies the electronic density of states at the Fermi level and causes an irregular change in the band structure energy. An important point is that none of the calculations suggests the correlation of the ETT with the special value of the axial ratio $c/a=\sqrt{3}$.

We are now left with the conclusion that the ETT may occur in Zn and Cd under high pressure and may produce some anomalies in the calculated volume dependence of the axial ratio, but the experimentally detected anomaly at $c/a=\sqrt{3}$ is never reproduced. We therefore have to consider other origins for this anomaly.

One of the alternative possibilities is a change in the lattice dynamical properties themselves of the hcp structure at $c/a=\sqrt{3}$. The anomaly in the Mössbauer spectra was also detected through the change in the lattice dynamics, which may not be necessarily connected to the ETT. This could be plausible, since what we observed in our x-ray experiments is an essential change in the slope of the volume dependence of the axial ratio, and is not an anomaly restricted to the vicinity of $c/a=\sqrt{3}$. In other words, the point $c/a=\sqrt{3}$ may simply represent a boundary between two kinds of hcp structures, which have different response to external pressures.[39] This hypothesis can be tested by studying, e.g., the phonon dispersion curves of the hcp structure as a function of the axial ratio, either experimentally or theoretically, and by looking for any distinct change at $c/a=\sqrt{3}$.[40]

Very recently Morgan *et al.* have reported the results of inelastic neutron scattering experiments on Zn under pressure at room temperature.[27] They observed a rapid hardening of a phonon frequency in the transverse acoustic branch Σ_3 starting at about 6.8 GPa. Unfortunately their measurements terminate just before the pressure for the c/a anomaly and offer no evidence for it. Nevertheless, the steep increase of the phonon frequency is indicative of the destruction of a

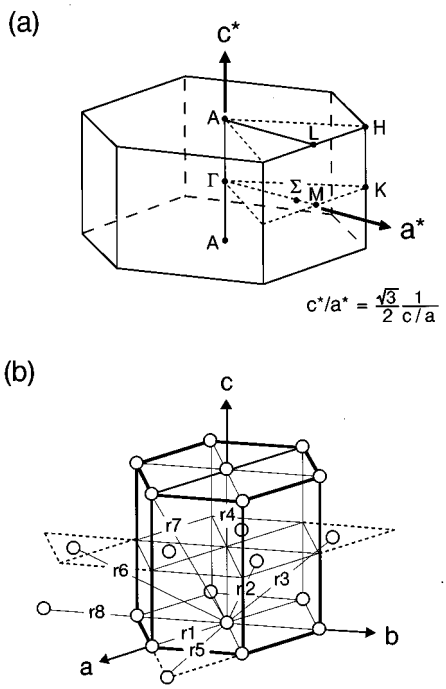

FIG. 14. (a) The first Brillouin zone for the hcp structure with symmetry points. The primitive vectors for the reciprocal lattice are shown by a^* and c^*. The ratio of c^* to a^* is given by $c^*/a^* = \sqrt{3}/2/(c/a)$. (b) The real lattice with interatomic distances. The interatomic distance r_j indicates the jth nearest neighbor distance for the case of the ideal hcp structure with $c/a = 1.633$.

giant Kohn anomaly at slightly higher pressures. Extension of the neutron scattering experiments to higher pressures is desirable, since we can directly compare the lattice dynamics with the structural change both at room temperature.

Another possible origin for the c/a anomaly is an hcp-to-hcp isostructural phase transition at $c/a = \sqrt{3}$. Since there is no detectable volume change at the pressure for the c/a anomaly, the phase transition could be of higher order. However, in the absence of any other experimental evidence regarding the phase change, we have to be careful to draw any conclusion at present. A crucial experiment to this point would be single-crystal x-ray diffraction on Zn under a truly hydrostatic condition.

C. Hcp structure with $c/a = \sqrt{3}$ and general remarks on the hcp metals

As noticed before, the c/a anomaly occurs exactly when a number of diffraction peaks simultaneously overlap. The overlap of diffraction peaks or coincidence of the d spacings indicates that the reciprocal lattice has special symmetry. Figure 14(a) shows the first Brillouin zone for the hcp structure. When $c/a = \sqrt{3}$, the $\Gamma\Gamma(=AA)$ and $\Gamma M(=AL)$ distances become equal, which results from the coincidence of the magnitude of [002] and [100] reciprocal lattice vectors.[41] Figure 14(b) shows the hcp structure in real space. For the axial ratio of $\sqrt{3}$ the interatomic distances r_4 and r_5 as well as r_7 and r_8 become equal. The hcp structure can also be represented by an orthorhombic unit cell (orthohexagonal cell) containing four atoms in it (Fig. 15). Since the interatomic distances r_4 and r_5 correspond to the length of the

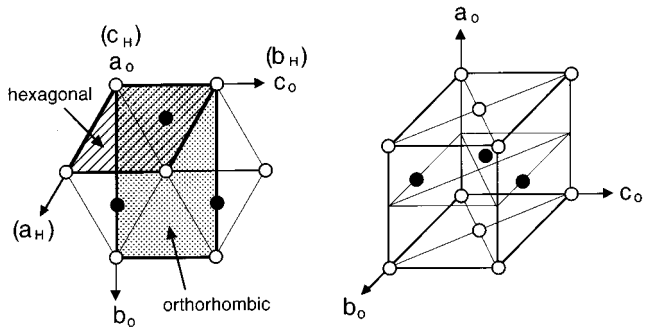

FIG. 15. The hcp structure with $c/a = \sqrt{3}$ in real space. The left figure shows a projection onto the (001) basal plane of the hexagonal system. Hexagonal and orthorhombic unit cells are indicated by different hatching. Lattice vectors a_0, b_0, and c_0 show the orthorhombic unit cell. The right figure shows a stereoscopic view of the orthorhombic cell.

a_0 and b_0 axes of the orthorhombic cell, the orthorhombic cell becomes tetragonal when the hexagonal axial ratio is $\sqrt{3}$.[42] In conclusion, the hcp structure with $c/a = \sqrt{3}$ has special symmetry both in real and reciprocal spaces, with which various distances are degenerate.

If we plot the Brillouin zone dimension of the hcp structure as a function of the c/a ratio, we notice another special point $c/a = 1.50$, where a similar degeneracy occurs to that at $c/a = \sqrt{3}$. For $c/a = 1.50$, the $\Gamma\Gamma$, ΓL, and ΓK distances are degenerate. As a result, regular hexagons appear in the planes perpendicular to the ΓK directions, having exactly the same shape as that in the basal plane.[41] This is the case for the high-pressure phase II of Ba, which exists between 5.5 and 12.6 GPa at room temperature.[43] Ba(II) has an hcp structure with the axial ratio of 1.58 at 5.5 GPa. The axial ratio dramatically decreases with pressure down to a value of 1.50 at 12.6 GPa. At this point Ba(II) transforms to the next high-pressure phase IV. We infer that the hcp structure may develop a kind of instability because of the special symmetry. Indeed the value of 1.50 is the smallest axial ratio ever found for the hcp structure, and possibly marks a lower limit for the stability region of the hcp structure. Compared to the points $c/a = 1.50$ and $\sqrt{3}$, no degeneracy occurs in the Brillouin zone dimension for the ideal hcp structure at $c/a = 1.633$. We recall that the volume dependence of the axial ratios of Zn and Cd shows no anomaly when the axial ratio passes through 1.633 (Fig. 8).

Figure 16 summarizes the axial ratios for the hcp elemental metals including hcp high-pressure phases. One notices that most of the hcp metals fall in the range $1.57 < c/a < 1.65$. Zn and Cd are exceptions at atmospheric pressure, but they also fall in this range of axial ratio at high pressures. According to the preceding discussions, we may classify the hcp structures into two groups: $1.50 < c/a < \sqrt{3}$ and $\sqrt{3} < c/a$. Zn and Cd transform from the latter group to the former one (normal hcp) under pressure.

Apart from high pressure, axial ratios of hcp metals can also be changed by alloying. There is a good correlation between the axial ratio and the electron concentration.[44] Cu-Zn, Au-Zn, Ag-Zn, and Ag-Cd alloys have hcp structures with large axial ratios in the Zn- or Cd-rich region (the η phase). The axial ratios of these alloys are, however, distrib-

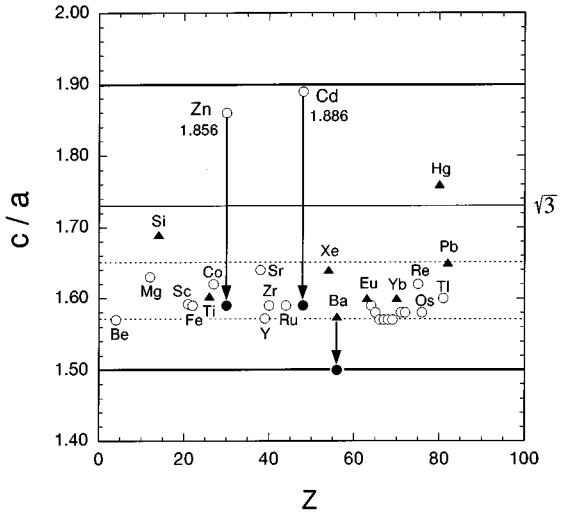

FIG. 16. The c/a axial ratios of hcp elemental metals as a function of atomic number. The open circles indicate the values at atmospheric pressure and the solid circles indicate those at high pressures. The solid triangles indicate the axial ratios of high-pressure phases at pressures where they appear. Unless specified, the variation of the c/a axial ratio with pressure is small. The thick solid lines indicate the upper and lower bounds for the axial ratios of known hcp structures. The axial ratios of most hcp metals fall in the range $1.57<c/a<1.65$ as indicated by the broken lines. A hypothetical boundary at $c/a=\sqrt{3}$ classifies the hcp structures into two groups.

uted in the range $1.75<c/a<1.87$, and no hcp alloy at normal pressure has an axial ratio in the range $1.65<c/a<1.75$.[45] Hcp structures having axial ratios in this region can only be obtained under high pressure. This could be a reason for long ignorance of the importance of the hcp structure with $c/a=\sqrt{3}$.

V. CONCLUSIONS

We have precisely determined the lattice parameters and the axial ratios of Zn and Cd under high pressure. The hcp phases are found to be stable over the whole pressure range studied. A clear change is observed in the slope of the volume dependence of the axial ratio at $c/a=\sqrt{3}$ for both metals. It seems difficult to connect the anomaly in the axial ratio to the electronic topological transition, since there is no reason for the ETT to occur at a special value of the axial ratio. Consideration of the hcp structure with $c/a=\sqrt{3}$ reveals interesting symmetry both in real and reciprocal spaces. A fundamental change may occur in the lattice dynamics and/or bonding properties of hcp metals at $c/a=\sqrt{3}$. If this hypothesis is true, hcp metals having axial ratios below and above this value should be classified into two different groups. Obviously further experimental and theoretical studies are necessary in order to elucidate the true origin for the anomaly presently found in the volume dependence of the axial ratios of Zn and Cd. These include measurements of transport properties, elastic constants, and phonon dispersion curves under high pressure. Single-crystal x-ray diffraction study under a very good hydrostatic condition would also be helpful. The bulk modulus and its pressure derivative are obtained as $B_0=65\pm2$ GPa and $B_0'=4.6\pm0.5$ for Zn, and $B_0=42\pm1$ GPa and $B_0'=6.5\pm0.2$ for Cd.

Note added in proof. The Cd-Mg alloy forms the hcp solid solution over the entire range of concentration at high temperatures. The change in the axial ratio with concentration has been determined at 310 °C [W. Hume-Rothery and G. V. Raynor, Proc. R. Soc. London, Ser. A **174**, 471 (1940)]. The axial ratio continuously changes from the value for pure Cd (1.900) to that for pure Mg (1.624), and hence passes through the value $\sqrt{3}$ at around 76% of the Cd concentration. No anomaly has been reported at this concentration.

ACKNOWLEDGMENTS

The author would like to thank Dr. N. Hamaya and Dr. H. Fujihisa for their help in the experiment on the beam line 14C. He also wishes to thank Dr. K. Terakura, Dr. K. Kobayashi, Dr. M. Arai, Dr. N. E. Christensen, Dr. O. Eriksson, Dr. B. K. Godwal, Dr. S. M. Sharma, Dr. V. V. Kechin, and Dr. S. Klotz for valuable discussions and communications. The present work has been done under the proposal Nos. 93G105 and 95G138 of the Photon Factory.

*Electronic address: takemura@nirim.go.jp

[1] W. A. Harrison, Phys. Rev. **129**, 2512 (1963).
[2] J. A. Moriarty, Phys. Rev. B **10**, 3075 (1974); **16**, 2537 (1977).
[3] J. Hafner and V. Heine, J. Phys. F **13**, 2479 (1983).
[4] D. Singh and D. A. Papaconstantopoulos, Phys. Rev. B **42**, 8885 (1990).
[5] R. W. Lynch and H. G. Drickamer, J. Phys. Chem. Solids **26**, 63 (1965).
[6] E. A. Perez-Albuerne, R. L. Clendenen, R. W. Lynch, and H. G. Drickamer, Phys. Rev. **142**, 392 (1966).
[7] H. Jones, Proc. R. Soc. London, Ser. A **147**, 396 (1934).
[8] J. B. Goodenough, Phys. Rev. **89**, 282 (1953).
[9] D. B. McWhan, J. Appl. Phys. **36**, 664 (1965).
[10] O. Schulte, A. Nikolaenko, and W. B. Holzapfel, High Pres. Res. **6**, 169 (1991).
[11] O. Schulte and W. B. Holzapfel, Phys. Rev. B **53**, 569 (1996).
[12] S. Meenakshi, V. Vijayakumar, B. K. Godwal, and S. K. Sikka, Phys. Rev. B **46**, 14 359 (1992).
[13] W. Potzel, M. Steiner, H. Karzel, W. Schiessl, M. Köfferlein, G. M. Kalvius, and P. Blaha, Phys. Rev. Lett. **74**, 1139 (1995).
[14] M. Steiner, W. Potzel, H. Karzel, W. Schiessl, M. Köfferlein, G. M. Kalvius, and P. Blaha, J. Phys. Condens. Matter **8**, 3581 (1996).
[15] K. Takemura, Phys. Rev. Lett. **75**, 1807 (1995).
[16] I. M. Lifshitz, Zh. Eksp. Teor. Fiz. **38**, 1569 (1960) [Sov. Phys. JETP 11, 1130 (1960)].
[17] See, for example, N. W. Ashcroft and N.D. Mermin, *Solid State Physics* (Holt-Saunders, Philadelphia, 1976), p. 169.
[18] W. A. Harrison, Phys. Rev. **118**, 1190 (1960).
[19] A good review on the electronic structures and the Fermi surfaces of Zn and Cd is found in S. Daniuk, T. Jarlborg, G. Kontrym-Sznajd, J. Majsnerowski, and H. Stachowiak, J. Phys. Condens. Matter **1**, 8397 (1989).
[20] K. Takemura, in *High Pressure Science and Technology, Pro-*

ceedings of the Joint XV AIRAPT and XXXIII EHPRG International Conference, Warsaw, 1995, edited by W. A. Trzeciakowski (World Scientific, Singapore, 1996), p. 748.

[21] O. Shimomura, K. Takemura, H. Fujihisa, Y. Fujii, Y. Ohishi, T. Kikegawa, Y. Amemiya, and T. Matsushita, Rev. Sci. Instrum. **63**, 967 (1992).

[22] I. Fujishiro, G. J. Piermarini, S. Block, and R. G. Munro, in *High Pressure in Research and Industry, Proceedings of the 8th AIRAPT Conference Uppsala*, edited by C. M. Backman, T. Johannisson, and L. Tegner (ISBN, Sweden, 1982), Vol. II, p. 608.

[23] H. K. Mao, P. M. Bell, J. W. Shaner, and D. J. Steinberg, J. Appl. Phys. **49**, 3276 (1978).

[24] J. Donohue, *The Structures of the Elements* (Wiley, New York, 1974), pp. 225–230.

[25] The nonhydrostatic data below 20 GPa are omitted in Tables I and II for clarity.

[26] S. N. Vaidya and G. C. Kennedy, J. Phys. Chem. Solids **31**, 2329 (1970).

[27] J. G. Morgan, R. B. Von Dreele, P. Wochner, and S. M. Shapiro, Phys. Rev. B **54**, 812 (1996).

[28] A. K. Singh, J. Appl. Phys. **73**, 4278 (1993).

[29] R. W. Stark and L. M. Falicov, Phys. Rev. Lett. **19**, 795 (1967).

[30] P. Blaha, K. Schwarz, and P. H. Dederichs, Phys. Rev. B **38**, 9368 (1988).

[31] D. F. Gibbons and L. M. Falicov, Philos. Mag. **86**, 177 (1963).

[32] O. L. Steenhaut and R. G. Goodrich, Phys. Rev. B **1**, 4511 (1970).

[33] E. S. Itskevich and A. N. Voronovskii, Sov. Phys. JETP Lett. **4**, 154 (1966) [Zh. Eksp. Teor. Fiz. Pis'ma Red. **4**, 226 (1966)].

[34] S. L. Bud'ko, A. N. Voronovskii, A. G. Gapotchenko, and E. S. Itskevich, Zh. Eksp. Teor. Fiz. **86**, 778 (1984) [Sov. Phys. JETP **59**, 454 (1984)].

[35] T. Brudevoll and N. E. Christensen, Bull. Am. Phys. Soc. **41**, 717 (1996).

[36] O. Eriksson (private communication).

[37] B. K. Godwal (private communication).

[38] V. V. Kechin (private communication).

[39] In this respect we notice that the interplanar spacings d_{002} and d_{100}, which are directly related to the c and a axis, exchange at $c/a=\sqrt{3}$ as described in Sec. IV C.

[40] It should be noted that the Raman frequency of the TO mode of Zn shows a smooth increase with pressure up to 54 GPa at room temperature without any detectable anomaly [H. Olijnyk, High Pres. Res. **10**, 461 (1992)].

[41] The special symmetry of the hcp structure with $c/a=\sqrt{3}$ and 1.50 is also discussed by V. F. Degtyareva, in *Stability of Materials*, Vol. 355 of *NATO Advanced Study Institute, Series B: Physics*, edited by A. Gonis, P. E. A. Turchi, and J. Kudrnovsky (Plenum, New York, 1995), pp. 465–470.

[42] S. M. Sharma, S. K. Sikka, and R. Chidambaram, in *Recent Trends in High Pressure Research*, edited by A. K. Singh (Oxford & IBH, New Delhi, 1992), pp. 878–880.

[43] K. Takemura, Phys. Rev. B **50**, 16 238 (1994).

[44] T. B. Massalski, J. Phys. Radium **23**, 647 (1962).

[45] See, for example, P. Villars and L. D. Calvert, *Pearson's Handbook of Crystallographic Data for Intermetallic Phases*, 2nd ed. (ASM International, Materials Park, OH, 1991).